nature genetics

Distinct patterns of somatic genome alterations in lung adenocarcinomas and squamous cell carcinomas

Joshua D Campbell[1,2], Anton Alexandrov[3,4], Jaegil Kim[1], Jeremiah Wala[1,2], Alice H Berger[1,2], Chandra Sekhar Pedamallu[1,2], Sachet A Shukla[1,2], Guangwu Guo[1,2], Angela N Brooks[1,2], Bradley A Murray[1,2], Marcin Imielinski[1,2,5], Xin Hu[6], Shiyun Ling[6], Rehan Akbani[6], Mara Rosenberg[1], Carrie Cibulskis[1], Aruna Ramachandran[1,2], Eric A Collisson[7], David J Kwiatkowski[1,8], Michael S Lawrence[1], John N Weinstein[6], Roel G W Verhaak[6], Catherine J Wu[1,2], Peter S Hammerman[1,2], Andrew D Cherniack[1,2], Gad Getz[1,9], Cancer Genome Atlas Research Network[10], Maxim N Artyomov[3], Robert Schreiber[3], Ramaswamy Govindan[11], Matthew Meyerson[1,2,12]

To compare lung adenocarcinoma (ADC) and lung squamous cell carcinoma (SqCC) and to identify new drivers of lung carcinogenesis, we examined the exome sequences and copy number profiles of 660 lung ADC and 484 lung SqCC tumor–normal pairs. Recurrent alterations in lung SqCCs were more similar to those of other squamous carcinomas than to alterations in lung ADCs. New significantly mutated genes included *PPP3CA*, *DOT1L*, and *FTSJD1* in lung ADC, *RASA1* in lung SqCC, and *KLF5*, *EP300*, and *CREBBP* in both tumor types. New amplification peaks encompassed *MIR21* in lung ADC, *MIR205* in lung SqCC, and *MAPK1* in both. Lung ADCs lacking receptor tyrosine kinase–Ras–Raf pathway alterations had mutations in *SOS1*, *VAV1*, *RASA1*, and *ARHGAP35*. Regarding neoantigens, 47% of the lung ADC and 53% of the lung SqCC tumors had at least five predicted neoepitopes. Although targeted therapies for lung ADC and SqCC are largely distinct, immunotherapies may aid in treatment for both subtypes.

Lung cancer remains the leading cause of death from cancer around the world[1]. An estimated 221,000 new cases and 158,000 deaths from lung cancer occurred in the United States alone in 2015 (ref. 2). The two major histological classes are non-small-cell lung cancer (NSCLC) and small-cell lung cancer (SCLC). NSCLCs mostly comprise lung ADCs and lung SqCCs. These two NSCLC subtypes have both unique and shared clinical and histopathological characteristics. For example, whereas smoking is the major risk factor for both subtypes, approximately 10–15% of lung ADCs are observed in never-smokers[3]. Molecularly targeted therapies directed against receptor tyrosine kinases (RTKs) lead to dramatic responses in subsets of patients with lung ADCs harboring activating genomic alterations in the corresponding kinase genes, including *EGFR*, *ALK*, and *ROS1* (ref. 4). Other targeted therapies under current investigation are directed against activating alterations in the *MET*, *RET*, *NTRK1*, *NTRK2*, *ERBB2*, and *BRAF* kinases[4,5].

Recent efforts have focused on comprehensively characterizing the changes found in the genome, epigenome, transcriptome, and proteome in lung ADCs and SqCCs to discover new cancer driver genes that may be clinically actionable[6–8]. Identifying new cancer-related genes can be challenging because of the large number of passenger mutations that can accumulate from prolonged exposure to tobacco carcinogens and from inherent mutagenic processes such as aberrant activity of APOBEC cytidine deaminases[9]. Profiling larger numbers of samples within a tumor type and combining samples across tumor types can help overcome this problem, by providing the additional statistical power necessary to distinguish important genes mutated at a lower frequency than other genes with passenger mutations[10]. In addition, a comprehensive comparison of recurrently altered genes found in lung ADC and lung SqCC has not been performed. Such analyses may yield insights into the similarities and differences in carcinogenesis between the diseases and elucidate the degree to which common or distinct targeted and immunological therapeutic strategies can be used to treat each cancer type.

RESULTS

Comparison of somatically altered genes

To compare the somatic profiles of lung ADC and lung SqCC and to identify new genetic alterations, we studied 660 lung ADC–normal paired exome sequences (including 274 previously unpublished

[1]Cancer Program, Eli and Edythe L. Broad Institute of Harvard and MIT, Cambridge, Massachusetts, USA. [2]Department of Medical Oncology, Dana-Farber Cancer Institute, Boston, Massachusetts, USA. [3]Department of Pathology and Immunology, Washington University, St. Louis, Missouri, USA. [4]Computer Technologies Laboratory, ITMO University, St. Petersburg, Russia. [5]Molecular Pathology Unit, Massachusetts General Hospital, Charlestown, Massachusetts, USA. [6]Department of Bioinformatics and Computational Biology, University of Texas MD Anderson Cancer Center, Houston, Texas, USA. [7]Department of Medicine, University of California, San Francisco, San Francisco, California, USA. [8]Department of Medicine, Brigham and Women's Hospital, Boston, Massachusetts, USA. [9]Department of Pathology, Massachusetts General Hospital, Boston, Massachusetts, USA. [10]A full list of members and affiliations appears at the end of the paper. [11]Department of Medicine, Washington University School of Medicine, St. Louis, Missouri, USA. [12]Department of Pathology, Harvard Medical School, Boston, Massachusetts, USA. Correspondence should be addressed to M.M. (matthew_meyerson@dfci.harvard.edu) or R.G. (rgovinda@dom.wustl.edu).

Received 4 September 2015; accepted 12 April 2016; published online 9 May 2016; doi:10.1038/ng.3564

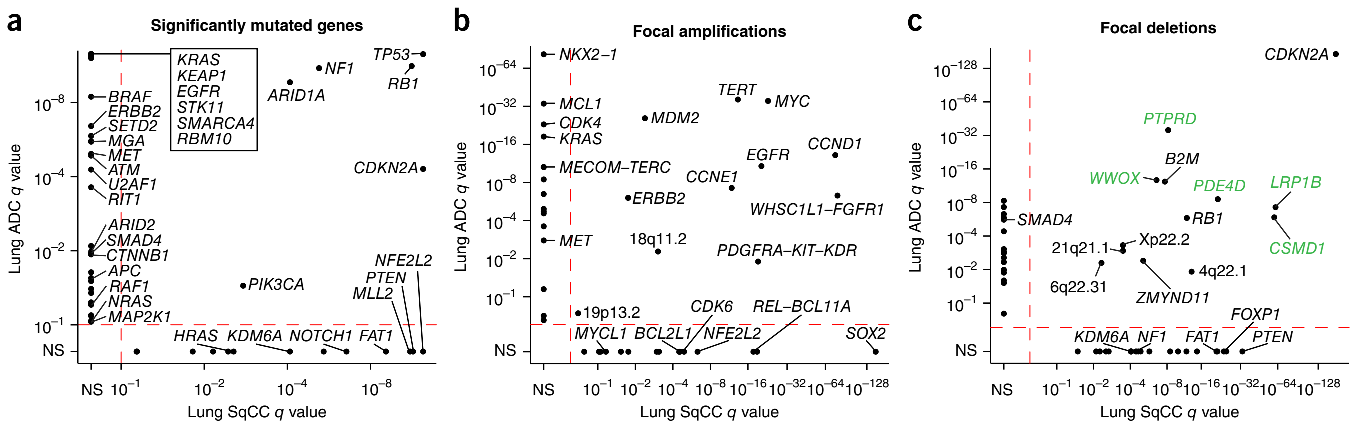

Figure 1 Distinct somatic alterations in lung ADC and lung SqCC. (**a**) The MutSig2CV algorithm[10] was used to identify significantly mutated genes across 660 lung ADCs and 484 lung SqCCs. Genes with q values <0.1 were considered to be significantly mutated. The q value for each gene in the lung ADC cohort is plotted against the respective q value in the lung SqCC cohort. The majority of significantly mutated genes were unique to either tumor type. (**b**,**c**) The GISTIC 2.0 algorithm was used to identify significantly recurrent copy number gains and losses. The q values for amplifications (**b**) and deletions (**c**) in the lung ADC cohort are plotted against the respective q values in the lung SqCC cohort. Peaks with q values <0.25 were considered to be significant. Deletions located within putative fragile sites are highlighted with green labels. Only points corresponding to genes with a previously characterized role in lung cancer are labeled. NS, not significant.

cases and 227 previously described cases from The Cancer Genome Atlas (TCGA)[6] together with 159 cases from the cohort in Imielinski *et al.*[8]) and 484 lung SqCC–normal paired exome sequences (including 308 previously unpublished cases and 176 previously described cases from TCGA[7]; **Supplementary Tables 1–4**). Similarly to previous studies[6,7], we observed median somatic mutation rates of 8.7 mutations/Mb and 9.7 mutations/Mb for lung ADCs and SqCCs, respectively. After excluding genes with lower median expression ($\log_2$ (FPKM) <6.16 for lung ADCs and <6.27 for lung SqCCs; Online Methods and **Supplementary Fig. 1**), we identified 38 genes as significantly mutated in lung ADC and 20 genes as significantly mutated in lung SqCC using MutSig2CV[10] (q value < 0.1; **Supplementary Tables 5** and **6**). Only six genes—*TP53*, *RB1*, *ARID1A*, *CDKN2A*, *PIK3CA*, and *NF1*—were significantly mutated in both tumor types, and, of these, *TP53*, *CDKN2A*, and *PIK3CA* had a significantly higher mutation frequency in lung SqCC tumors (P < 0.01, Fisher's exact test; **Fig. 1a**). Likewise, only 11 of 42 focal amplification peaks were identified as altered in both tumor types (**Fig. 1b**), and 13 of 50 focal deletion peaks were altered in both tumor types (**Fig. 1c**). Interestingly, when compared to 19 other tumor types from TCGA[10], the lists of significantly mutated genes for lung ADC and lung SqCC had greater overlap with lists of significantly mutated genes from other tumor types (>13% overlap; false discovery rate (FDR) q value < 0.1) than with each other (12% overlap; P = 0.105; **Supplementary Fig. 2**), consistent with previous pan-cancer analyses[11]. Recurrently mutated and amplified genes in lung SqCC most closely resembled the genes altered in head and neck squamous cell carcinoma (HNSC) and bladder cancer (BLCA), two other epithelial cancers with epidemiological associations with smoking (>25% overlap; **Supplementary Fig. 2**). Among these overlapping genes, *TP53*, *CDKN2A*, and *FAT1* are specifically enriched for alterations in human papillomavirus (HPV)-negative HNSC[12]. In contrast, the significantly mutated genes in lung ADC were most similar to those in glioblastoma (GBM) and colorectal cancer (CRC) (FDR q value < 0.1). Although lung ADC and lung SqCC did share several focal deletion peaks, five of these peaks are putative fragile sites (shown in green in **Fig. 1c**). Taken together, these results suggest that the somatic drivers of carcinogenesis may be largely distinct in lung ADC and lung SqCC.

Mutational signatures in lung cancer

Various carcinogenic and cancer-related processes contribute to the mutational patterns observed in tumors[13,14]. Previous large-scale studies of lung cancer genomes have identified signatures associated with non-smoking and smoking cases[6,8,15]; here we extend these findings through the improved statistical power of our larger sample set. Using non-negative matrix factorization (NMF)[13,16] (Online Methods), we identified six mutational signatures in this cohort, many of which are strongly correlated with previously defined signatures in the Catalogue of Somatic Mutations in Cancer (COSMIC) database[13,17] (**Supplementary Figs. 3–5** and **Supplementary Table 7**). These included a UV-related signature of C>T changes at T$\underline{\text{C}}$C or C$\underline{\text{C}}$C sites (COSMIC signature 7, abbreviated SI7), a smoking-related signature of C>A transversions (SI4), a mismatch-repair (MMR) signature of C>T changes at G$\underline{\text{C}}$G sites (SI15/SI6), two APOBEC-related signatures of C>G or C>T changes at T$\underline{\text{C}}$T or T$\underline{\text{C}}$A sites (SI13 and SI2), and a final signature with a moderate correlation to COSMIC signature 5 (SI5) with putative 'molecular clock' properties[18] (**Supplementary Fig. 5**). In addition to identifying mutational signatures, NMF also estimates the number of mutations contributed by each signature in each tumor. The estimated number of SI4 (smoking-related) mutations per megabase displayed a bimodal pattern in lung ADC but not in lung SqCC (**Fig. 2a**). Furthermore, the rate of SI4 mutations per megabase was able to classify tumors into those from never- versus ever-smokers substantially better in lung ADC (area under the curve (AUC) = 0.87; **Supplementary Fig. 6**) than in lung SqCC (AUC = 0.62), suggesting that the smoking statuses for the 18 never-smokers with lung SqCC may be inaccurate. Eighty-seven percent of lung ADCs from never-smokers were categorized as transversion low (≤0.696 SI4 mutations/Mb; $P = 8.5 \times 10^{-37}$, Fisher's exact test; **Fig. 2b** and **Supplementary Fig. 6**). However, only 45% of transversion-low lung ADCs were from patients who were never-smokers (**Fig. 2b**). For each tumor, we also derived the fraction of estimated mutations for a signature by dividing the number of estimated mutations for that signature by the sum of estimated mutations from all signatures. Lung SqCCs displayed significantly higher overall rates of SI5 mutations per megabase when compared to all lung ADCs (P < 0.001, Wilcoxon rank-sum test). However, lung ADCs from never-smokers displayed the highest fraction of estimated mutations

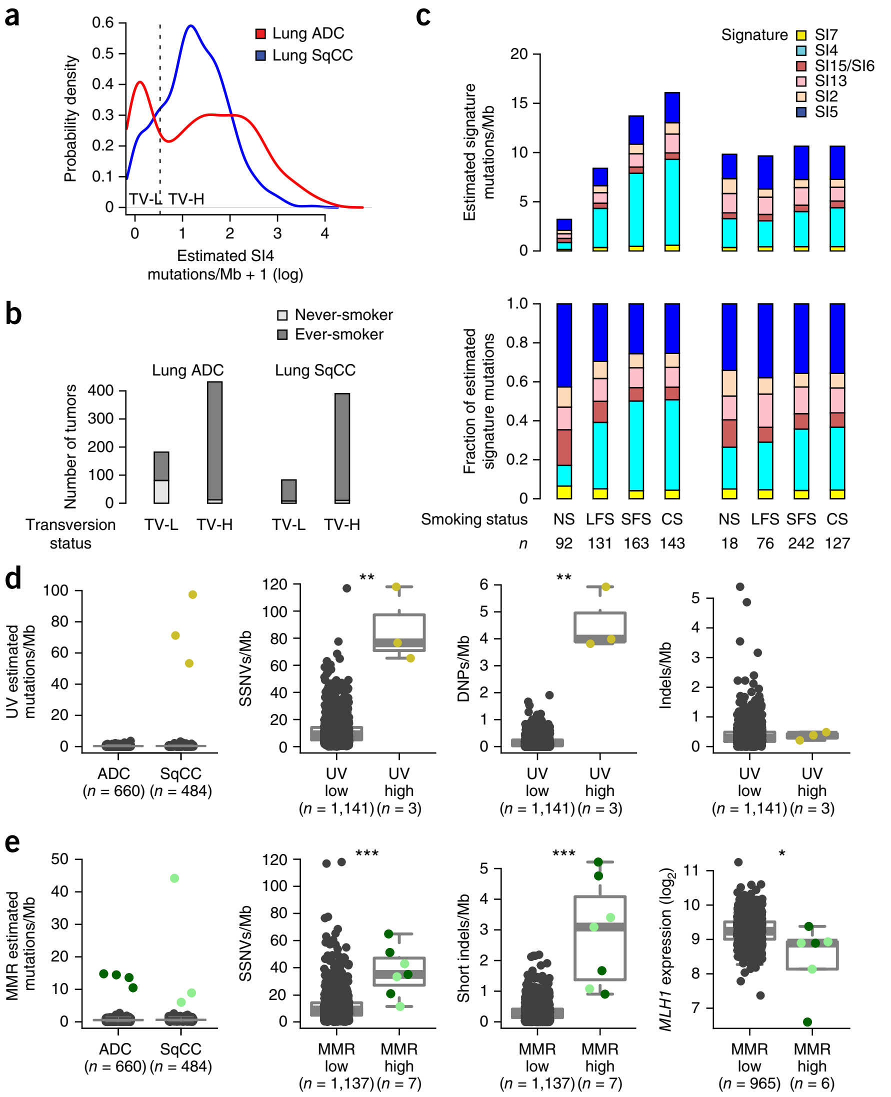

Figure 2 Comparison of mutational signatures in lung cancer. Six mutational signatures were identified using NMF on 192 distinct mutation types. (**a**) The estimated number of SI4 (smoking-related) mutations per megabase in each tumor displayed a bimodal pattern in lung ADC (red). TV-L, transversion low; TV-H, transversion high. (**b**) Lung ADCs categorized as transversion low were enriched for clinically annotated lifelong never-smokers ($P = 8.5 \times 10^{-37}$). (**c**) The estimated number of mutations for each signature per megabase (top) and the fraction of estimated mutations for each signature (bottom) were averaged across lifelong never-smokers (NS), longer-term former smokers (LFS), shorter-term former smokers (SFS), and current smokers (CS) for both lung ADCs and lung SqCCs (excluding the UV-high and MMR-high tumors discussed below). (**d**) Three lung SqCCs had a high number of estimated mutations from a UV-associated signature commonly observed in melanoma. These tumors displayed a significantly higher overall rate of SSNVs and DNPs when compared to all other lung tumors ($P < 0.01$). (**e**) The mutational profiles for another seven tumors exhibited an MMR-like signature commonly observed in MSI CRCs. These tumors had significantly higher rates of both SSNVs and short indels ($P < 0.001$), as well as lower levels of *MHL1* expression ($P = 0.011$). Asterisks indicate significance levels from Wilcoxon rank-sum tests: $^*P < 0.05$, $^{**}P < 0.01$, $^{***}P < 0.001$. Each boxplot shows the median (middle bar), first quartile (bottom of the box), and third quartile (top of the box). Boxplot whiskers demark 1.5 times the interquartile range or minimum–maximum values.

from this signature on average (**Fig. 2c** and **Supplementary Fig. 7**). In lung SqCC, we also observed moderate associations of tumor stage with SI5 activity and total mutation rate ($P < 0.01$; **Supplementary Fig. 8**).

The mutational profiles of three lung SqCCs (~1% of lung SqCCs) exhibited a pattern of UV-related mutations (SI7) commonly observed in melanoma and displayed a significantly higher mutation rate of somatic single-nucleotide variants (SSNVs) and somatic dinucleotide polymorphisms (DNPs) when compared to the other lung tumors ($P < 0.01$) but not higher rates of indels ($P > 0.05$; **Fig. 2d**). One of these patients (TCGA-18-3409) had a previous history of basal cell carcinoma in the forehead, raising the possibility that metastasis from the skin to the lung had occurred. The other two lung SqCCs with this signature may also represent squamous cell skin carcinomas metastatic to the lung. The mutational profiles for another seven tumors (four lung ADCs and three lung SqCCs) exhibited an MMR-like signature (SI15/SI6) commonly observed in CRCs with microsatellite instability (MSI) (**Fig. 2e**)[13]. These tumors had significantly higher rates of both SSNVs and short indels when compared to all other lung tumors with expression data ($P < 0.001$). They also displayed lower expression levels of the MMR gene *MLH1* ($P = 0.011$), suggesting a potential etiology for this signature in lung.

New significantly mutated genes

Comparing the significantly mutated genes to those in other tumor types from TCGA Pan-Cancer study[10] showed that there were several genes significantly mutated exclusively in lung ADC, including *STK11*, *RBM10*, *KEAP1*, *RAF1*, *RIT1*, and *MET* (MutSig2CV *q* value < 0.1; **Fig. 3a** and **Supplementary Table 5**). *NFE2L2*, *KDM6A*, *RASA1*, *NOTCH1*, and *HRAS* were significantly mutated in lung SqCC but not in other cancer types (excluding HNSC and BLCA) (**Fig. 3b** and **Supplementary Table 6**). Genes that reached modest statistical significance in lung ADC that have been observed previously to be altered in lung cancer or in other tumor types included *AKT1*, with a recurrent mutation encoding p.Glu17Lys, *CDK4*, with a recurrent mutation encoding p.Arg24Leu, and *DNMT3A* ($P < 0.005$; **Supplementary Table 5**). The new significantly mutated genes exclusive to lung ADC and which are not altered in other tumor types included *PPP3CA*, which encodes the catalytic subunit for the calcium-dependent phosphatase, calcineurin. The mutations in *PPP3CA* clustered in the sequence encoding the autoinhibitory domain near the C terminus of the protein, suggesting that they may be gain-of-function alterations (**Fig. 4a**). In addition, mutations mapping to the autoinhibitory domain also tended to co-occur with activating *KRAS* mutations ($P = 0.033$), suggesting a potential relationship between the K-Ras and calcineurin signaling pathways. Significantly mutated methyltransferase genes included *MLL3* (*KMT2C*) and *SETD2*. A new gene in this class was the H3K79 methyltransferase *DOT1L*, which was mutated

Figure 3 Significantly mutated genes in lung cancer as compared to other cancer types. (**a**) The *q* value for each significantly mutated gene in the lung ADC cohort is plotted against the best *q* value for the same gene in 19 other tumor types from a pan-cancer study[10]. (**b**) The *q* values from the lung SqCC cohort were similarly compared to those from the other tumor types, excluding HNSC and BLCA. The size of each point is proportional to the frequency of mutations in the gene. The color of the point indicates enrichment for mutation clustering as defined by MutSig2CV ($-\log_{10}$ (P_{CL})) and/or enrichment for loss-of-function mutations ($-\log_{10}$ (*P* value)) as determined with a Fisher's exact test (Online Methods). Black points in the lower-right quadrants represent genes significantly mutated in another cancer type but not in lung ADC and/or lung SqCC.

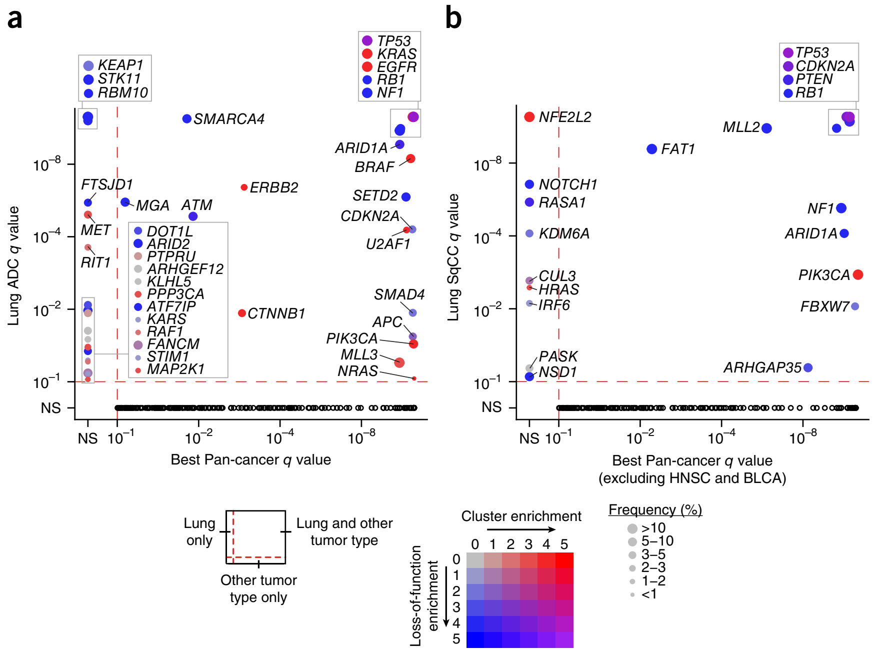

in 3% of lung ADCs with enrichment for truncating mutations (**Fig. 4a**). Recurrent mutations in lung ADC have previously been reported in splicing factors such as *U2AF1*, and loss-of-function mutations have been identified in the RNA-binding protein *RBM10* (ref. 8). In the current data set, a cap methyltransferase, *FTSJD1* (also known as *CMTR2*), was significantly mutated and enriched for frameshift mutations (**Fig. 4a**). We also examined genes for other known proteins in this class and found recurrent mutations in *SF3B1* (ref. 19) and *SNRPD3* (**Supplementary Fig. 9**). *EGFR* mutations were enriched in females, and *SMARCA4* mutations were enriched in males (FDR *q* value < 0.1; **Supplementary Table 8**). *RBM10* mutations were modestly enriched in males, as previously reported (*q* value = 0.219)[6]. The new significantly mutated genes in lung SqCC that were enriched for frameshift mutations ($P < 0.001$) included *RASA1*, whose protein product is p120GAP[20] (**Fig. 4b**). *CUL3*, whose protein product is a known interaction partner of KEAP1, also reached statistical significance in the lung SqCC cohort[21] (**Fig. 4b**). *RB1* mutations were enriched in females, whereas *PASK* mutations were exclusive to males (FDR *q* value < 0.1; **Supplementary Table 9**). We did not observe significant associations between mutation status and patient survival or tumor stage after correction for multiple-hypothesis testing (**Supplementary Tables 10–13**). Controlling for tumor stage did not identify additional significant associations between mutation status and survival.

Previous studies have shown that joint analysis of different tumor types can yield additional statistical power to detect low-frequency events, even if the tumor types are from vastly different tissues of origin and/or etiologies[10]. Additionally, although the individual drivers may be distinct between two tumor types, pathways such as mitogen-activated protein (MAP) kinase signaling are often altered similarly in both. We therefore hypothesized that combining the lung ADC and lung SqCC tumor cohorts (into a pan-lung cohort) would identify additional recurrent somatic pathway alterations common to both tumor types. We found 14 genes significantly mutated in the pan-lung cohort that were not significantly mutated in either individual tumor type (*q* value < 0.1; **Supplementary Fig. 10** and **Supplementary Table 14**). Many of these genes are involved in epigenetic regulation or immune-related pathways. *KLF5*, a transcription factor critical for lung development[22], contained a new recurrent mutation mapping to the zinc-finger domain, which was observed in both ADCs and SqCCs (**Fig. 4c**). A regulator of *KLF5*, the E3 ubiquitin ligase *FBXW7* (ref. 23), was also significantly mutated in the lung SqCC and pan-lung cohorts but did not co-occur with *KLF5* mutations. A super-enhancer duplication associated with increased *KLF5* expression has also recently been reported in HNSC by our group[24], and *KLF5* has been reported to be recurrently mutated in BLCA[25]. The paralogs *EP300* and *CREBBP* had a mutational hotspot region mapping to the histone acetyltransferase (HAT) domain. All missense mutations mapping to the HAT domain and other loss-of-function alterations outside this domain were non-overlapping for these two proteins. For sites with sufficient sequencing depth in the RNA-seq analysis (power >95%), we observed an SSNV validation rate of 88%.

New somatic copy number alterations

With a larger sample size, we had better resolution to detect new copy number changes and ascertain the putative target genes of focal amplifications and deletions. For some peaks that still contained many genes, we inferred the most likely target gene by examining the same peak in a pan-cancer copy number analysis across 11 tumor types[26] that included a subset of the lung cancers from this set. The most significantly focally amplified genes in lung ADC were *NKX2-1*, *MYC*, *TERT*, *MCL1*, and *MDM2* (**Fig. 5a** and **Supplementary Table 15**), and peaks at *SOX2*, *CCND1*, *WHSC1L1–FGFR1*, *MYC*, and *EGFR* were among the most significant for lung SqCC (**Fig. 5b** and **Supplementary Table 16**). Amplification peaks previously described in other tumor types but less characterized in lung tumors included *KAT6A*, *ZNF217*, and *MYCL1* for lung ADC (**Fig. 5a**) and *IGF1R*, *KDM5A*, *PTP4A1–PHF3*, and *MYCL1* for lung SqCC (**Fig. 5b**). *CCND3* was specifically amplified in lung ADC, whereas an amplification peak near *MIR21–TUBD1* (**Fig. 5c**) was also observed in breast cancer[26]. *MIR21* expression has been shown to be a prognostic factor for early-stage ADC[27,28]. Likewise, new amplification peaks for lung SqCC included *YES1*, encoding a Src family non-receptor protein kinase, and *MIR205* (**Fig. 5d**). Expression of *MIR205* has been used to distinguish lung SqCCs from other NSCLC types[29], suggesting that amplification of this microRNA (miRNA) may represent a lineage-specific alteration similar to *SOX2* amplification. Finally, combined pan-lung copy number analysis identified additional amplification peaks around *MAPK1* (**Fig. 5a–d** and **Supplementary Table 17**).

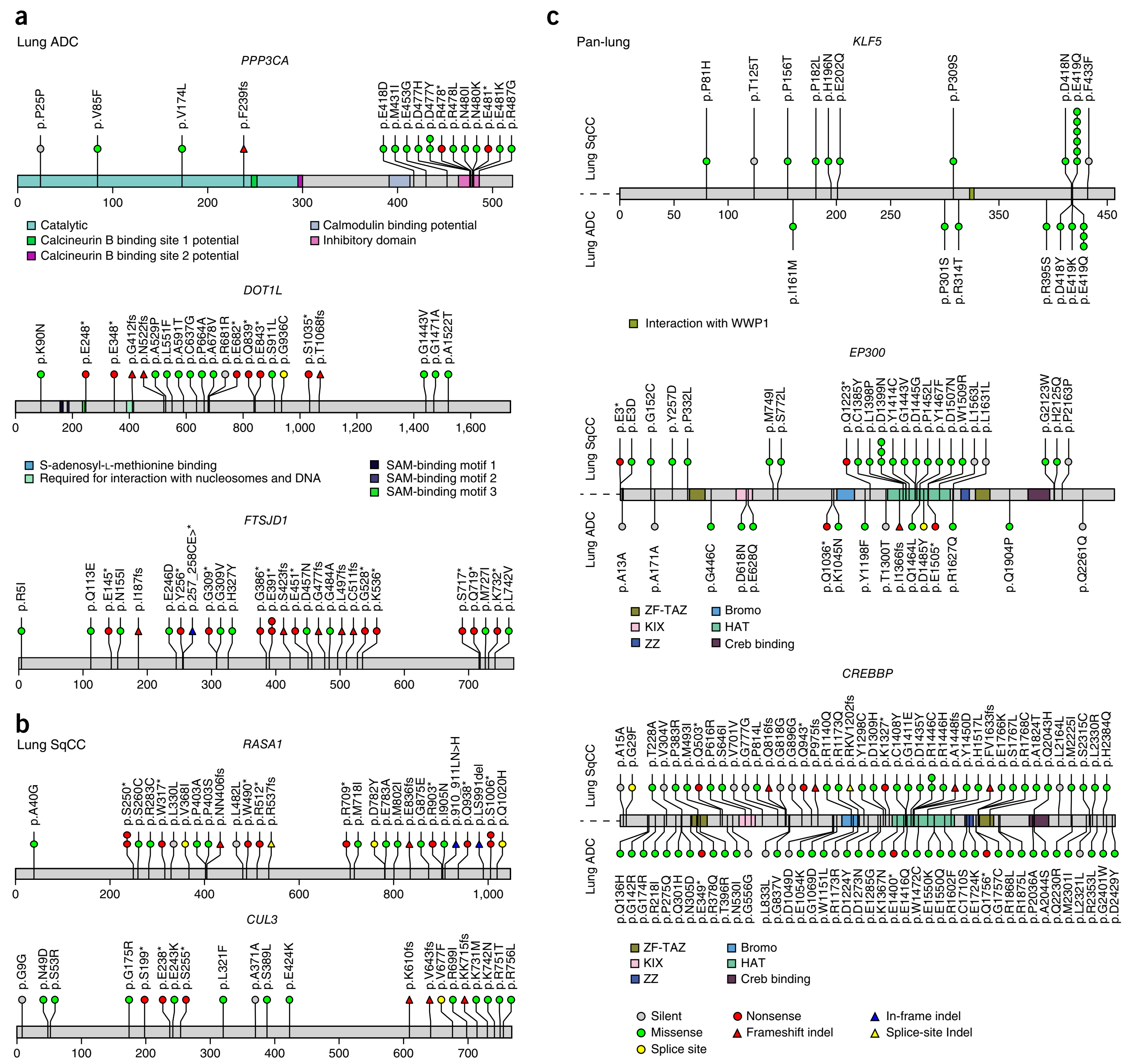

Figure 4 New significantly mutated genes in lung cancer. (**a**,**b**) Alteration profiles are shown for new genes specific to each lung tumor type, including *PPP3CA*, *DOT1L*, and *FTSJD1* for lung ADC (**a**) and *RASA1* and *CUL3* for lung SqCC (**b**). (**c**) Combined (pan-lung) analysis of both tumor types identified additional significantly mutated genes with hotspots, including *KLF5* and two paralogs, *EP300* and *CREBBP*.

Focal deletion peaks in lung ADC included the chromatin modifier genes *SMARCA4* and *ARID2* (**Supplementary Fig. 11** and **Supplementary Table 18**), which were also significantly mutated and enriched for loss-of-function mutations. New lung SqCC focal deletions observed in other tumor types included *ZMYND11*, *CREBBP*, *ROBO1*, *USP22*, and *KDM6A* (**Supplementary Fig. 11** and **Supplementary Table 19**). *B2M* (β2 microglobulin), encoding a component of the MHC complex, was focally deleted in both tumor types, was enriched for loss-of-function mutations in both tumor types ($P < 0.01$), and was significantly mutated in the pan-lung analysis (FDR q value = 0.006). Combined pan-lung copy number analysis identified another focal deletion peak around *TRAF3* (**Supplementary Table 20**), which was also reported in HNSC[12]. In general, mRNA expression was significantly associated ($P < 0.05$) with copy number levels for target genes (**Supplementary Figs. 12** and **13**). We did not observe substantial batch effects within or across tumor types in either the mRNA expression or copy number variation data (**Supplementary Figs. 14** and **15**).

Identifying RTK–Ras–Raf drivers in lung ADC

In lung ADC, mutually exclusive alterations have been characterized in components of the RTK–Ras–Raf signaling pathway. These alterations are of particular interest because of the dramatic responses that have been observed to RTK inhibitors in clinical trials such as those for patients with lung ADC harboring *EGFR* mutation or *ALK* or *ROS1* translocations[30]. However, many lung ADCs do not exhibit a known

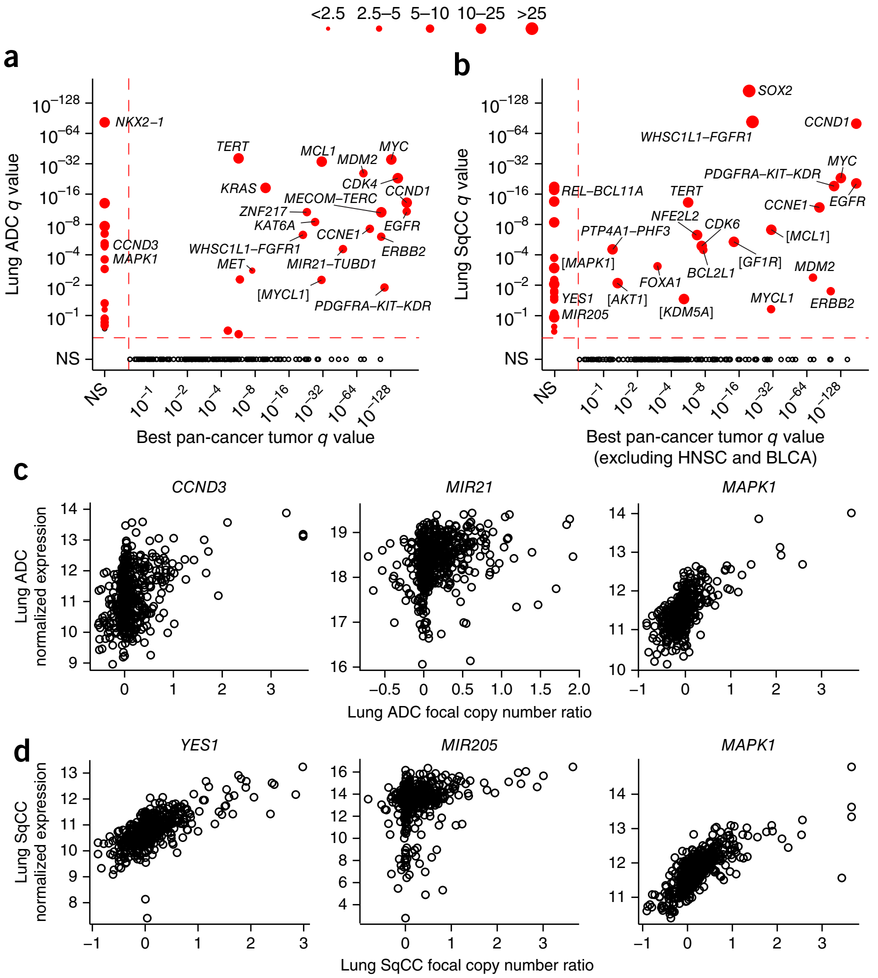

Figure 5 Significant amplifications in lung cancer. (**a**) The *q* value for each amplification peak in lung ADC is plotted against the best *q* value for the same region across nine other non-lung tumor types[26]. (**b**) The *q* values for amplification peaks in lung SqCC are compared against seven other tumor types, excluding HNSC and BLCA. The size of each point is proportional to the frequency of focal amplification. Brackets around gene names indicate that the most likely target gene was inferred from pan-cancer copy number analysis across 11 tumor types or from the combined pan-lung copy number analysis. Black points in the lower-right quadrants indicate genes significantly altered by amplifications in another cancer type but not in lung ADC and/or lung SqCC. (**c**,**d**) Gene expression is plotted against focal copy number ratios for new amplification peaks that include *CCND3*, *MIR21*, and *MAPK1* in lung ADC (**c**) and *YES1*, *MIR205*, and *MAPK1* in lung SqCC (**d**).

activating mutation in the pathway, raising the possibility that additional genes with low-frequency somatic events are yet to be identified. To further understand the somatic landscape of this pathway, we first characterized alterations among known pathway members and then identified new genes with mutually exclusive alterations. New alterations in known pathway genes included a recurrent in-frame insertion in *MAP2K1* and a fusion of *MET* with its neighboring gene, *CAPZA2* (**Fig. 6** and **Supplementary Table 21**)[31]. Previously reported *TRIM24–NTRK2* and *KIF5B–MET* fusions[31] were observed in tumors without other known activating alterations. Interestingly, another *NTRK2* fusion with *TP63* was also found in a lung SqCC (**Fig. 6** and **Supplementary Table 21**). As observed previously, high levels of *MET* and *ERBB2* amplification were enriched in tumors without other known activating alterations in this pathway ($P < 0.01$; **Supplementary Fig. 16**)[6]. A single lung ADC (TCGA-49-4512) harbored an activating *EGFR* alteration resulting in kinase domain duplication[32]. By manual review, we found additional canonical mutations in *KRAS*, *EGFR*, or *ERBB2* in 17 tumors and complex indels in *EGFR* or *MET* in 11 tumors, some of which have been previously reported[6,8,33] (**Supplementary Table 22**).

Lung ADCs that had an activating SSNV, indel, amplification, or gene fusion affecting a known RTK–Ras–Raf driver[6,34,35] were designated 'oncogene positive' ($n = 418$), whereas the remaining lung ADCs were considered 'oncogene negative' ($n = 242$). For the purposes of this analysis, we did not include *NF1*-altered tumors in the oncogene-positive group, as mutations in this gene are not entirely mutually exclusive with alterations in other genes related to the RTK–Ras–Raf pathway. To identify additional potential drivers in this pathway, we determined whether genes that were significantly mutated in any of the MutSig2CV analyses (**Supplementary Tables 5**, **6**, and **14**) or that are important in regulation of the Ras pathway[36] were enriched for alterations in oncogene-negative samples using a Fisher's exact test. In total, 15 genes were significantly enriched for alterations among oncogene-negative samples, including the known Ras pathway components *SOS1* and *RASA1* and the Rho kinase pathway components *VAV1* and *ARHGAP35* (q value < 0.1; **Fig. 7a**,**c** and **Supplementary Table 23**). SOS1 is a guanine-nucleotide-exchange factor (GEF) bound to the RTK complex and assists in the activation of Ras proteins[37]. Recurrent mutations were observed encoding a p.Asn233Tyr substitution in the autoinhibitory domain (DH) of SOS1 in four lung ADCs, and the p.Asp309Tyr substitution in the same region has been reported in Noonan syndrome[38,39] (**Supplementary Fig. 17**). Similarly, VAV1 is a GEF for the Rho family GTPases. Interactions between the calponin homology (CH), acidic (Ac), and pleckstrin homology (PH) domains are important for autoinhibition of the catalytic Dbl homology domain[40]. The p.Ser67Tyr substitution is located near the interface of the CH, Ac, and PH domains, and mutagenesis affecting this site has been shown to increase overall GEF activity[40] (**Supplementary Fig. 17**). *RASA1* and *ARHGAP35* (p190RhoGAP) encode GTPase-activating proteins (GAPs) for the Ras and Rho kinases, respectively, and were each enriched for loss-of-function mutations ($P < 0.01$). We also identified amplification peaks near *FGFR1–WHSC1L1* (8p11.21), *PDGFRA–KIT–KDR* (4q12), and *MAPK1* (22q11) that were only significant in the oncogene-negative tumor set (q value < 0.25; **Fig. 7b**,**c**). In total, 499 (76%) lung ADCs displayed an alteration in known or putative RTK–Ras–Raf driver genes (**Fig. 7c**). Moreover, 193 of 227 (85%) lung ADCs that previously underwent secondary expert pathological review and had RNA-seq data available for fusion analysis[6] harbored a predicted activating alteration in the RTK–Ras–Raf pathway.

New co-occurrences included *MET* amplifications and *NF1* mutations ($P = 0.019$; **Supplementary Fig. 16**). Additionally, high-level *EGFR* amplification significantly overlapped with activating *EGFR*

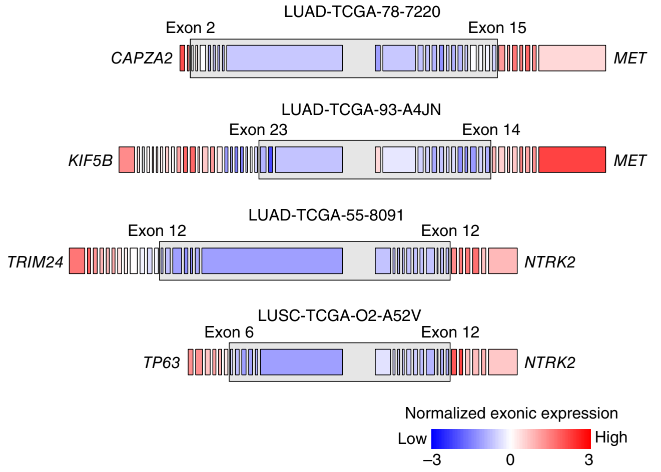

Figure 6 Fusions involving *MET* and *NTRK2*. Two fusions of *MET* were identified that retained the sequence encoding the RTK domain, including one with its neighboring gene, *CAPZA2*. This fusion most likely arose via tandem duplication resulting in the 3′ end of *MET* being fused with the 5′ end of *CAPZA2*. Previously reported *TRIM24*–*NTRK2* and *KIF5B*–*MET* fusions[31] were observed in lung ADCs without other known activating alterations in RTK–Ras–Raf signaling. Another *NTRK2* fusion with *TP63* was also found in a lung SqCC. For each fusion, the expression of exons retained in the putative fusion transcript was relatively higher than the expression of exons not in the putative fusion transcript (as indicated by the gray box).

mutations ($P = 1.9 \times 10^{-8}$)[41,42], and *STK11* mutations significantly overlapped with activating *KRAS* mutations ($P = 1.1 \times 10^{-6}$; **Fig. 7c**)[43,44]. Furthermore, 28 lung ADCs that remain oncogene negative for the RTK–Ras–Raf pathway harbored *STK11* mutations (**Fig. 7c**), suggesting the possibility of an additional, hitherto unrecognized *KRAS*-related genome alteration complementary to *STK11* mutation in these cancer samples.

Assessment of neoantigen load and recurrence

Because of the increasing interest in the use of immune checkpoint inhibitors in lung cancer[45,46], we comprehensively analyzed the potential immunogenic properties of the mutational landscape. For each patient, we evaluated the ability of the protein sequence resulting from each somatic missense mutation to be processed and presented to immune cells by any one of the patient-specific HLA alleles[47,48]. We then assessed the association between the number of immunogenic mutations (resulting in neoepitopes or neoantigens) and clinical characteristics and identified the most common neoepitopes observed in lung cancer. Both nonsynonymous mutation and neoepitope counts were not significantly different between lung ADCs and lung SqCCs from ever-smokers (**Fig. 8a**,**b**). However, these counts were significantly lower in lung ADCs from never-smokers in comparison to lung ADCs from ever-smokers ($P < 0.001$, Wilcoxon rank-sum test; **Fig. 8a**,**b**) and were associated with overall smoking history

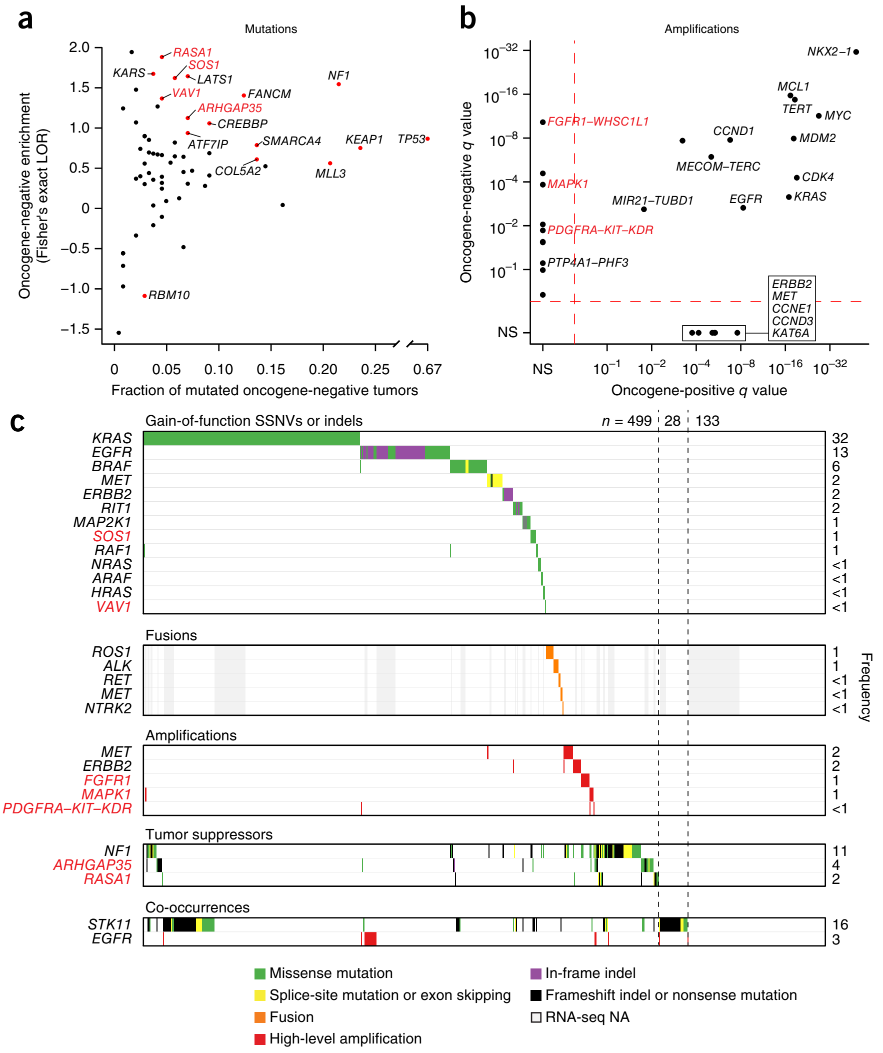

Figure 7 New alterations in the RTK–Rho/Ras–Raf pathway in lung ADC. Lung ADCs were classified as oncogene positive if they harbored a known activating or recurrent alteration in previously characterized pathway components and were classified as oncogene negative otherwise. (**a**) Fifteen genes (red points) were significantly enriched for mutations among oncogene-negative tumors (Fisher's exact test, FDR *q* value < 0.1; **Supplementary Table 23**). A log-transformed odds ratio (LOR) greater than 0 indicates that the frequency of mutations was higher in the oncogene-negative set. (**b**) Significant amplification peaks near *FGFR1*–*WHSC1L1*, *PDGFRA*–*KIT*–*KDR*, and *MAPK1* were only found in the oncogene-negative tumor set using GISTIC 2.0 (*q* value < 0.25). (**c**) Co-mutation plot for known and new activators of the pathway. Tumors were considered to have high-level amplification for a given gene if they had a total $\log_2$-transformed copy number ratio greater than 1. For genes with gain-of-function SSNVs or indels, only recurrently mutated sites or sites with previous experimental functional evidence were included. New genes enriched for alterations among oncogene-negative tumors that are members of the RTK–Rho/Ras–Raf pathway are labeled in red in all panels. Dashed lines separate tumors that harbor a known or putative alteration in this pathway (*n* = 499), tumors that do not harbor an alteration in this pathway but have a mutation in *STK11* (*n* = 28), and tumors that do not harbor an alteration in this pathway or *STK11* (*n* = 133). NA, RNA-seq data were not available.

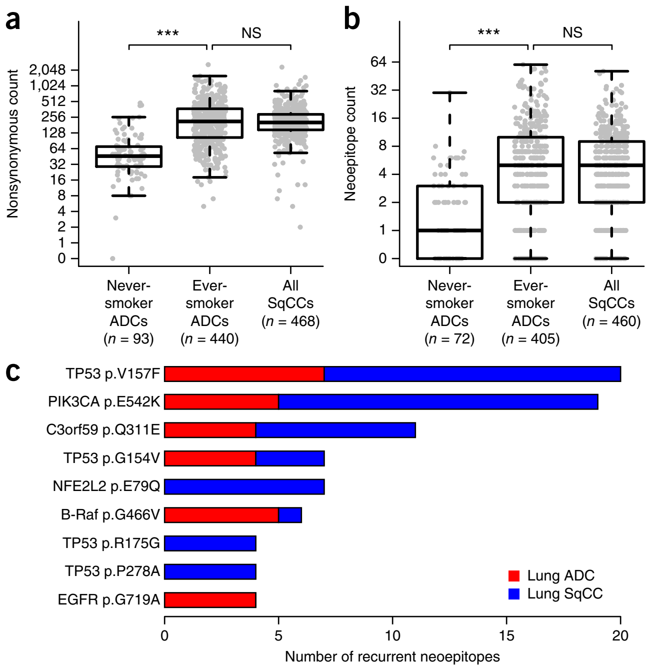

Figure 8 Neoepitope load in lung cancer. The immunogenicity of each missense mutation was predicted after inferring HLA alleles in each tumor with available RNA-seq data. (**a**,**b**) Nonsynonymous mutation counts (**a**) and neoepitope counts (**b**) were not significantly different between ever-smokers from lung ADCs and lung SqCCs ($P > 0.05$). However, these counts were significantly lower in lung ADCs from never-smokers than in lung ADCs from ever-smokers (***$P < 0.001$). (**c**) Some of the most common alterations predicted to be neoepitopes included TP53 p.Val157Phe, PIK3CA p.Glu542Lys, and C3orf59 p.Gln311Glu.

in lung ADCs but not lung SqCCs ($P < 0.001$, Kruskal–Wallis test; **Supplementary Fig. 18**). Alterations predicted to generate neoepitopes in at least four tumors included PIK3CA p.Glu542Lys, NFE2L2 p.Glu79Gln, B-Raf p.Gly466Val, EGFR p.Gly719Ala, and several alterations in TP53, including p.Val157Phe, p.Gly154Val, p.Arg175Gly, and p.Pro278Ala (**Fig. 8c**). A gene not previously implicated in lung cancer, *C3orf59* (also known as *MB21D2*), harbored a recurrent mutation encoding p.Gln311Glu, which has predicted neoepitope properties (**Fig. 8c**). Overall, 47% of lung ADC and 53% of lung SqCC samples had at least five predicted neoepitopes, suggesting great potential for immunotherapy.

DISCUSSION

We examined the exome sequences and copy number profiles of 1,144 lung cancers to explore similarities and differences between lung ADC and lung SqCC. Consistent with studies of gene expression[11], this comparison showed that both mutated genes and recurrent somatic copy number alterations are largely distinct for the two lung cancer types. The similarity between lung SqCCs, HNSCs, and a subset of BLCAs was also observed when 12 tumor types were reclassified using clustering of five molecular data types[11]. These differences suggest that somatic alterations can have different oncogenic potential in different cellular contexts. Thus, cancers arising from developmentally similar cells of origin across different tissues will be more similar than cancers arising from different cells of origin within an anatomically defined tissue. As we had only one tumor sample per patient, we were not able to analyze intratumoral heterogeneity, as has been done in other studies[49,50].

Several new focal amplification peaks containing protein-coding genes, including *MAPK1*, *YES1*, and *CCND3*, were identified. Interestingly, we also found two peaks that contained or were near miRNA genes (*MIR21* in lung ADC and *MIR205* in lung SqCC). We have also recently reported the duplication of a noncoding super-enhancer that results in increased *MYC* expression[24]. As the mutational analyses in this study focused on whole-exome sequencing of protein-coding genes, we were not able to examine mutations in noncoding genes or regulatory elements. Future studies examining large numbers of whole genomes from lung cancer may be better suited for discovery of other oncogenic alterations in noncoding genes or regulatory elements.

Our study has uncovered multiple significantly mutated genes in the RTK–Ras–Raf pathway, including newly identified genes such as *RASA1*, *SOS1*, and *VAV1*. Previous studies examining smaller numbers of lung tumors were not able to detect recurrent mutations in *SOS1* (refs. 8,39). The fact that we were able to detect these mutants further highlights the usefulness of increasing sample size to detect rare events. Because we did not have matching RNA-seq data for every tumor, we may be underestimating the rates of oncogenic fusions or *MET* exon 14 skipping events. As 15–25% of lung ADCs still do not have a known, detectable alteration in the RTK–Ras–Raf pathway, we may yet be underpowered to find additional rare, recurrent mutations in known and new pathway components. Similar considerations may be relevant for other pathways. For example, we identified new epigenetic modifier mutations in *CREBBP* and *EP300*, previously shown in SCLC[51].

Finally, we examined the immunogenicity of individual missense mutations to understand more fully the association between neoepitope loads, overall nonsynonymous mutation rates, and clinical variables such as smoking status. Some highly recurrent mutations were predicted to result in neoepitopes. Future studies may further unravel the relationship between these candidates and clinical responses to immune checkpoint inhibitors and customized vaccine therapies.

URLs. Picard tools, http://broadinstitute.github.io/picard/; MutSig algorithm, http://www.broadinstitute.org/cancer/cga/MutSig; Indelocator, http://www.broadinstitute.org/cancer/cga/indelocator; Broad Institute Firehose pipeline, http://www.broadinstitute.org/cancer/cga/; Oncotator, http://www.broadinstitute.org/oncotator/; power calculations, http://www.tumorportal.org/; PRADA fusions, http://www.tumorfusions.org/; mutational signatures, http://www.mathworks.com/matlabcentral/fileexchange/38724; University of California Santa Cruz Cancer Genomics Hub, http://cghub.ucsc.edu/; TCGA Data Portal, http://tcga-data.nci.nih.gov/tcga/; Pan-Lung Tumor Portal, http://pubs.broadinstitute.org/panlung/.

METHODS

Methods and any associated references are available in the online version of the paper.

Accession codes. Binary alignment (BAM) files for all TCGA samples[6,7] can be downloaded from the University of California Santa Cruz Cancer Genomics Hub using the UUIDs in **Supplementary Table 2**. Additional clinical and molecular data for TCGA samples can be accessed via the TCGA Data Portal (see URLs).

Note: Any Supplementary Information and Source Data files are available in the online version of the paper.

ACKNOWLEDGMENTS
This work was supported by grants from the National Cancer Institute as part of The Cancer Genome Atlas project: U24CA126546, U24CA143867, U24CA143845,

U24CA126544, and U24CA143883. Additionally, this work was funded by National Cancer Institute grant K08CA163677 (P.S.H.), grant 074-U01 from the government of the Russian Federation (A.A.), US Department of Defense contract W81XWH-12-1-0269 (M.M.), the American Cancer Society Research Professor Award (M.M.), and National Cancer Institute grant R35CA197568 (M.M.).

AUTHOR CONTRIBUTIONS

J.D.C. performed sample quality control, mutation calling and review, ABSOLUTE analysis of tumors from the cohort of Imielinski *et al.*, identification and comparison of recurrently altered genes, mutational signature identification and characterization, identification of *EGFR* complex indels, and manuscript writing. A.A., M.N.A., and R.S. generated neoantigen calls. J.K. contributed to mutational signature analyses. J.W. contributed to *EGFR* complex indel characterization. A.H.B. contributed to oncogene-negative analysis and manuscript preparation. C.S.P. generated the pan-lung portal. A.N.B. identified *MET* exon 14 skipping events using RNA-seq. X.H. and R.G.W.V. generated fusion calls. S.L. and R.A. performed batch effect analyses. G. Guo contributed to *MET* exon 14 complex indel identification. M.R., M.I., M.S.L., and G. Getz contributed algorithms for mutation calling and analyses. B.A.M. and A.D.C. contributed to copy number and ABSOLUTE analyses. S.A.S. and C.J.W. performed HLA genotyping. C.C. contributed to sample coordination and quality control. A.R., A.D.C., E.A.C., J.N.W., P.S.H., and D.J.K. contributed to manuscript preparation. R.G. and M.M. conceived and designed the study and wrote the manuscript.

COMPETING FINANCIAL INTERESTS

The authors declare competing financial interests: details are available in the online version of the paper.

Reprints and permissions information is available online at http://www.nature.com/reprints/index.html.

1. Stewart, B.W. & Wild, C.P. *World Cancer Report 2014* (International Agency for Research on Cancer, 2014).
2. Siegel, R.L., Miller, K.D. & Jemal, A. Cancer statistics, 2015. *CA Cancer J. Clin.* **65**, 5–29 (2015).
3. Samet, J.M. *et al.* Lung cancer in never smokers: clinical epidemiology and environmental risk factors. *Clin. Cancer Res.* **15**, 5626–5645 (2009).
4. Cardarella, S. & Johnson, B.E. The impact of genomic changes on treatment of lung cancer. *Am. J. Respir. Crit. Care Med.* **188**, 770–775 (2013).
5. Vaishnavi, A. *et al.* Oncogenic and drug-sensitive *NTRK1* rearrangements in lung cancer. *Nat. Med.* **19**, 1469–1472 (2013).
6. Cancer Genome Atlas Research Network. Comprehensive molecular profiling of lung adenocarcinoma. *Nature* **511**, 543–550 (2014).
7. Cancer Genome Atlas Research Network. Comprehensive genomic characterization of squamous cell lung cancers. *Nature* **489**, 519–525 (2012).
8. Imielinski, M. *et al.* Mapping the hallmarks of lung adenocarcinoma with massively parallel sequencing. *Cell* **150**, 1107–1120 (2012).
9. Roberts, S.A. *et al.* An APOBEC cytidine deaminase mutagenesis pattern is widespread in human cancers. *Nat. Genet.* **45**, 970–976 (2013).
10. Lawrence, M.S. *et al.* Discovery and saturation analysis of cancer genes across 21 tumour types. *Nature* **505**, 495–501 (2014).
11. Hoadley, K.A. *et al.* Multiplatform analysis of 12 cancer types reveals molecular classification within and across tissues of origin. *Cell* **158**, 929–944 (2014).
12. Cancer Genome Atlas Network. Comprehensive genomic characterization of head and neck squamous cell carcinomas. *Nature* **517**, 576–582 (2015).
13. Alexandrov, L.B. *et al.* Signatures of mutational processes in human cancer. *Nature* **500**, 415–421 (2013).
14. Lawrence, M.S. *et al.* Mutational heterogeneity in cancer and the search for new cancer-associated genes. *Nature* **499**, 214–218 (2013).
15. Govindan, R. *et al.* Genomic landscape of non–small cell lung cancer in smokers and never-smokers. *Cell* **150**, 1121–1134 (2012).
16. Alexandrov, L.B., Nik-Zainal, S., Wedge, D.C., Campbell, P.J. & Stratton, M.R. Deciphering signatures of mutational processes operative in human cancer. *Cell Reports* **3**, 246–259 (2013).
17. Forbes, S.A. *et al.* COSMIC: exploring the world's knowledge of somatic mutations in human cancer. *Nucleic Acids Res.* **43**, D805–D811 (2015).
18. Alexandrov, L.B. *et al.* Clock-like mutational processes in human somatic cells. *Nat. Genet.* **47**, 1402–1407 (2015).
19. Quesada, V. *et al.* Exome sequencing identifies recurrent mutations of the splicing factor *SF3B1* gene in chronic lymphocytic leukemia. *Nat. Genet.* **44**, 47–52 (2012).
20. Bernards, A. GAPs galore! A survey of putative Ras superfamily GTPase activating proteins in man and *Drosophila*. *Biochim. Biophys. Acta* **1603**, 47–82 (2003).
21. Hast, B.E. *et al.* Cancer-derived mutations in *KEAP1* impair NRF2 degradation but not ubiquitination. *Cancer Res.* **74**, 808–817 (2014).
22. Wan, H. *et al.* Kruppel-like factor 5 is required for perinatal lung morphogenesis and function. *Development* **135**, 2563–2572 (2008).
23. Zhao, D., Zheng, H.Q., Zhou, Z. & Chen, C. The Fbw7 tumor suppressor targets KLF5 for ubiquitin-mediated degradation and suppresses breast cell proliferation. *Cancer Res.* **70**, 4728–4738 (2010).
24. Zhang, X. *et al.* Identification of focally amplified lineage-specific super-enhancers in human epithelial cancers. *Nat. Genet.* **48**, 176–182 (2016).
25. Cancer Genome Atlas Research Network. Comprehensive molecular characterization of urothelial bladder carcinoma. *Nature* **507**, 315–322 (2014).
26. Zack, T.I. *et al.* Pan-cancer patterns of somatic copy number alteration. *Nat. Genet.* **45**, 1134–1140 (2013).
27. Akagi, I. *et al.* Combination of protein coding and noncoding gene expression as a robust prognostic classifier in stage I lung adenocarcinoma. *Cancer Res.* **73**, 3821–3832 (2013).
28. Saito, M. *et al.* The association of microRNA expression with prognosis and progression in early-stage, non–small cell lung adenocarcinoma: a retrospective analysis of three cohorts. *Clin. Cancer Res.* **17**, 1875–1882 (2011).
29. Lebanony, D. *et al.* Diagnostic assay based on hsa-miR-205 expression distinguishes squamous from nonsquamous non-small-cell lung carcinoma. *J. Clin. Oncol.* **27**, 2030–2037 (2009).
30. Oxnard, G.R., Binder, A. & Jänne, P.A. New targetable oncogenes in non-small-cell lung cancer. *J. Clin. Oncol.* **31**, 1097–1104 (2013).
31. Stransky, N., Cerami, E., Schalm, S., Kim, J.L. & Lengauer, C. The landscape of kinase fusions in cancer. *Nat. Commun.* **5**, 4846 (2014).
32. Gallant, J.N. *et al.* EGFR kinase domain duplication (EGFR-KDD) is a novel oncogenic driver in lung cancer that is clinically responsive to afatinib. *Cancer Discov.* **5**, 1155–1163 (2015).
33. Ye, K. *et al.* Systematic discovery of complex insertions and deletions in human cancers. *Nat. Med.* **22**, 97–104 (2016).
34. Pao, W. & Girard, N. New driver mutations in non-small-cell lung cancer. *Lancet Oncol.* **12**, 175–180 (2011).
35. Pao, W. & Hutchinson, K.E. Chipping away at the lung cancer genome. *Nat. Med.* **18**, 349–351 (2012).
36. Stephen, A.G., Esposito, D., Bagni, R.K. & McCormick, F. Dragging Ras back in the ring. *Cancer Cell* **25**, 272–281 (2014).
37. Rajalingam, K., Schreck, R., Rapp, U.R. & Albert, S. Ras oncogenes and their downstream targets. *Biochim. Biophys. Acta* **1773**, 1177–1195 (2007).
38. Lepri, F. *et al.* *SOS1* mutations in Noonan syndrome: molecular spectrum, structural insights on pathogenic effects, and genotype–phenotype correlations. *Hum. Mutat.* **32**, 760–772 (2011).
39. Swanson, K.D. *et al.* *SOS1* mutations are rare in human malignancies: implications for Noonan syndrome patients. *Genes Chromosom. Cancer* **47**, 253–259 (2008).
40. Yu, B. *et al.* Structural and energetic mechanisms of cooperative autoinhibition and activation of Vav1. *Cell* **140**, 246–256 (2010).
41. Shan, L. *et al.* Concurrence of *EGFR* amplification and sensitizing mutations indicate a better survival benefit from EGFR-TKI therapy in lung adenocarcinoma patients. *Lung Cancer* **89**, 337–342 (2015).
42. Sholl, L.M. *et al.* Lung adenocarcinoma with *EGFR* amplification has distinct clinicopathologic and molecular features in never-smokers. *Cancer Res.* **69**, 8341–8348 (2009).
43. Liu, Y. *et al.* Metabolic and functional genomic studies identify deoxythymidylate kinase as a target in *LKB1*-mutant lung cancer. *Cancer Discov.* **3**, 870–879 (2013).
44. Kim, H.S. *et al.* Systematic identification of molecular subtype–selective vulnerabilities in non-small-cell lung cancer. *Cell* **155**, 552–566 (2013).
45. Brahmer, J. *et al.* Nivolumab versus docetaxel in advanced squamous-cell non–small-cell lung cancer. *N. Engl. J. Med.* **373**, 123–135 (2015).
46. Rizvi, N.A. *et al.* Mutational landscape determines sensitivity to PD-1 blockade in non–small cell lung cancer. *Science* **348**, 124–128 (2015).
47. Shukla, S.A. *et al.* Comprehensive analysis of cancer-associated somatic mutations in class I HLA genes. *Nat. Biotechnol.* **33**, 1152–1158 (2015).
48. Gubin, M.M. *et al.* Checkpoint blockade cancer immunotherapy targets tumour-specific mutant antigens. *Nature* **515**, 577–581 (2014).
49. Zhang, J. *et al.* Intratumor heterogeneity in localized lung adenocarcinomas delineated by multiregion sequencing. *Science* **346**, 256–259 (2014).
50. de Bruin, E.C. *et al.* Spatial and temporal diversity in genomic instability processes defines lung cancer evolution. *Science* **346**, 251–256 (2014).
51. Peifer, M. *et al.* Integrative genome analyses identify key somatic driver mutations of small-cell lung cancer. *Nat. Genet.* **44**, 1104–1110 (2012).

Collaborators:

Jean C Zenklusen[13], Jiashan Zhang[13], Ina Felau[13], John A Demchok[13], Liming Yang[13], Zhining Wang[13], Martin L Ferguson[13], Roy Tarnuzzer[13], Carolyn M Hutter[13], Heidi J Sofia[13], Todd Pihl[14], Yunhu Wan[14], Sudha Chudamani[15], Jia Liu[15], Charlie Sun[14], Rashi Naresh[14], Laxmi Lolla[15], Ye Wu[15], Chad J Creighton[16], W Kimryn Rathmell[17], J Todd Auman[17,18], Saianand Balu[19], Tom Bodenheimer[19], D Neil Hayes[19,20], Katherine A Hoadley[19,21], Alan P Hoyle[19], Corbin D Jones[22,23], Stuart R Jefferys[19], Shaowu Meng[19], Piotr A Mieczkowski[21], Lisle E Mose[19], Charles M Perou[18,19,21], Jeffrey Roach[24], Yan Shi[19], Janae V Simons[19], Tara Skelly[21], Matthew G Soloway[19], Donghui Tan[21], Junyuan Wu[19], Umadevi Veluvolu[21], Joel S Parker[19,21], Matthew D Wilkerson[21], Lori Boice[17,25], Mei Huang[17,25], Leigh B Thorne[18,19,25], Gad Getz[1,9], Michael S Noble[1], Hailei Zhang[1], David I Heiman[1], Juok Cho[1], Nils Gehlenborg[1,26], Gordon Saksena[1], Doug Voet[1], Pei Lin[1], Scott Frazer[1], Jaegil Kim[1], Michael S Lawrence[1], Lynda Chin[1,27], Ming-Sound Tsao[28], Frances Allison[28], Dianne Chadwick[28], Thomas Muley[29,30], Michael Meister[29,30], Hendrik Dienemann[29,30], Raju Kucherlapati[31,32], Peter Park[31,32], Jay Bowen[33], Julie M Gastier-Foster[33,34], Mark Gerken[33], Kristen M Leraas[33], Tara M Lichtenberg[33], Nilsa C Ramirez[33,34], Lisa Wise[33], Erik Zmuda[33], Josh Stuart[35], Eric Collisson[7], Martin Peifer[36,37], David Kwiatkowski[1,8], Joshua D Campbell[1,2], Bradley A Murray[1,2], Andrew D Cherniack[1,2], Alice H Berger[1,2], Carrie Sougnez[1], Steven E Schumacher[1,38], Juliann Shih[1,2], Rameen Beroukhim[1,2,39], Travis I Zack[1,38], Stacey B Gabriel[1], Matthew Meyerson[1,2,12], Lauren A Byers[40], Tanja Davidsen[13], Peter W Laird[41], Daniel J Weisenberger[42], David J Van Den Berg[42], Moiz S Bootwalla[42], Phillip H Lai[42], Dennis T Maglinte[42], Stephen B Baylin[43], James G Herman[44], Ludmila Danilova[43], Leslie Cope[43], Daniel J Crain[45], Erin Curley[45], Johanna Gardner[45], Kevin Lau[45], David Mallery[45], Scott Morris[45], Joeseph Paulauskis[45], Robert Penny[45], Candace Shelton[45], Troy Shelton[45], Mark Sherman[45], Peggy Yena[45] & Gordon B Mills[46]

[13]National Cancer Institute, US National Institutes of Health, Bethesda, Maryland, USA. [14]SRA International, Fairfax, Virginia, USA. [15]Leidos Biomedical, Rockville, Maryland, USA. [16]Baylor College of Medicine, Houston, Texas, USA. [17]University of North Carolina at Chapel Hill, Chapel Hill, North Carolina, USA. [18]Department of Pathology and Laboratory Medicine, School of Medicine, University of North Carolina at Chapel Hill, Chapel Hill, North Carolina, USA. [19]Lineberger Comprehensive Cancer Center, University of North Carolina at Chapel Hill, Chapel Hill, North Carolina, USA. [20]Department of Internal Medicine, University of North Carolina at Chapel Hill, Chapel Hill, North Carolina, USA. [21]Department of Genetics, University of North Carolina at Chapel Hill, Chapel Hill, North Carolina, USA. [22]Department of Biology, University of North Carolina at Chapel Hill, Chapel Hill, North Carolina, USA. [23]Carolina Center for Genome Sciences, University of North Carolina at Chapel Hill, Chapel Hill, North Carolina, USA. [24]Research Computing Center, University of North Carolina at Chapel Hill, Chapel Hill, North Carolina, USA. [25]University of North Carolina Tissue Procurement Facility, Chapel Hill, North Carolina, USA. [26]Center for Biomedical Informatics, Harvard Medical School, Boston, Massachusetts, USA. [27]Department of Genomic Medicine, University of Texas MD Anderson Cancer Center, Houston, Texas, USA. [28]University Health Network and Princess Margaret Cancer Centre, Toronto, Ontario, Canada. [29]Thoraxklinik am Universitätsklinikum Heidelberg, Heidelberg, Germany. [30]Translational Lung Research Centre Heidelberg, German Centre for Lung Research, Heidelberg, Germany. [31]Harvard Medical School, Boston, Massachusetts, USA. [32]Brigham and Women's Hospital, Boston, Massachusetts, USA. [33]Research Institute at Nationwide Children's Hospital, Columbus, Ohio, USA. [34]The Ohio State University, Columbus, Ohio, USA. [35]Department of Biomolecular Engineering, University of California, Santa Cruz, Santa Cruz, California, USA. [36]Department of Translational Genomics, Cologne, Germany. [37]Center for Molecular Medicine Cologne, Cologne, Germany. [38]Department of Cancer Biology, Dana-Farber Cancer Institute, Boston, Massachusetts, USA. [39]Department of Medicine, Harvard Medical School, Boston, Massachusetts, USA. [40]Department of Thoracic Head and Neck Medical Oncology, MD Anderson Cancer Center, Houston, Texas, USA. [41]Center for Epigenetics, Van Andel Research Institute, Grand Rapids, Michigan, USA. [42]Norris Comprehensive Cancer Center, University of Southern California, Los Angeles, California, USA. [43]Sidney Kimmel Comprehensive Cancer Center, Johns Hopkins University, Baltimore, Maryland, USA. [44]Hillman Cancer Center, University of Pittsburgh Cancer Institute, Pittsburgh, Pennsylvania, USA. [45]International Genomics Consortium, Phoenix, Arizona, USA. [46]Department of Systems Biology, University of Texas MD Anderson Cancer Center, Houston, Texas, USA.

ONLINE METHODS

Sample collection and pathology review. Sample collection and DNA sequencing were performed for the Imielinski *et al.* and TCGA cohorts as previously described[6–8]. All specimens were obtained from patients with appropriate consent and with approval from the relevant institutional review boards. All patients were naive to treatment with the exception of four patients with lung SqCC and three patients with lung ADC who received neoadjuvant treatment before resection (**Supplementary Table 2**). Initial pathological review was performed at the contributing tissue source sites, where each tumor was given an initial histological classification. After shipment of the frozen tissue to the Biospecimen Core Resource (BCR), one or two additional frozen sections were cut and stained with hematoxylin and eosin to confirm the histological classification of the original tissue source site. 159 of the lung ADCs from Imielinski *et al.*, 289 of the lung ADCs from TCGA, and 213 of the lung SqCCs from TCGA had also undergone additional histological review by an expert pathology committee led by W. Travis (Memorial Sloan Kettering Cancer Center) in previous studies[6–8]. Nucleic acid extraction and molecular quality control were performed at the BCR.

DNA sequencing, alignment, and mutation calling. Exome capture was performed using the Agilent SureSelect Human All Exon 50Mb kit followed by Illumina paired-end sequencing. Reads were processed using the Picard pipeline[6]. This pipeline uses BWA for read alignment, Picard tools for marking duplicates, and the Genome Analysis Toolkit (GATK) for realignment around small indels as well as recalibration of base quality[52]. Contamination in tumor exomes was estimated using ContEst[53]. Only tumors with <5% contamination, an available SNP6.0 array for copy number analysis, and a valid ABSOLUTE[54] solution were considered in the final analysis. The final sample set included 227 previously described lung ADCs from TCGA[6], 274 newly reported lung ADCs from TCGA, and 159 lung ADCs from the cohort of Imielinski *et al.*[8], together with 176 previously described lung SqCCs from TCGA[7] and 308 newly reported lung SqCCs from TCGA. SSNVs and indels were called using MuTect[55] and Indelocator (see URLs), respectively. These algorithms compare the tumor to the matched normal sample to exclude germline variants. Somatic calls were excluded if found in a panel of over 2,900 normal exomes, as previously described[10]. Coding mutation patterns can be viewed for individual genes in the Pan-Lung Tumor Portal (see URLs).

Identification of significantly mutated genes. Significantly mutated genes were identified using MutSig2CV, which combines P values from tests for high mutational frequency relative to the background mutation rate (P_{CV}), clustering of mutations within a gene (P_{CL}), and enrichment of mutations at evolutionarily conserved sites (P_{FN})[10]. For 660 lung ADCs, we had 100% power to detect genes mutated in 10% of patients and 73% power to detect genes mutated in 5% of patients, assuming a mutation rate of 8.7 mutations/Mb[10]. For 484 lung SqCCs, we had 100% power to detect genes mutated in 10% of patients and 41% power to detect genes mutated in 5% of patients, assuming a mutation rate of 9.7 mutations/Mb[10]. To reduce the number of hypotheses tested in the MutSig2CV analysis, we excluded genes that exhibited low expression across tumors with relatively high purity. The median $\log_2$ (FPKM) value for each gene was obtained for 185 ADCs and 238 SqCCs that had a purity estimate from ABSOLUTE of >50% and available RNA-seq data (**Supplementary Fig. 1**). For each tumor type, a mixture model of two normal distributions was fit in R using the mclust package v4.2. Genes with 95% probability of belonging to the cluster with higher expression were considered in multiple-hypothesis correction of the MutSig2CV combined P values. One gene, *TRERF1*, was excluded from the final results because closer inspection of its mutations showed a recurrent frameshift deletion that was likely a false positive, as all of these mutations had low allelic fractions (<1.5%) and had no supporting reads in matching RNA-seq data. A one-sided Fisher's exact test was used to determine whether the ratio of loss-of-function mutations (including nonsense, frameshift, and *de novo* out-of-frame start codon mutations) to other mutations for a given gene was significantly higher than the ratio of loss-of-function mutations to other mutations across all other genes.

Identification of recurrent copy number changes. DNA was hybridized onto Affymetrix SNP6.0 arrays, and signal intensities were normalized as previously described[6]. Segmentation was performed using the Circular Binary Segmentation algorithm[56] followed by Ziggurat Deconstruction to infer the length and amplitude of each segment. Recurrent peaks for focal somatic copy number alteration were identified using GISTIC 2.0 (ref. 57). A peak was considered to be focally amplified or deleted within a tumor if the GISTIC 2.0–estimated focal copy number ratio was greater than 0.1 or less than −0.1, respectively. Purity and ploidy were estimated using ABSOLUTE[54]. Two peaks were considered the same across tumor types if (i) the known target gene of each peak was the same or (ii) the genomic location of the peaks overlapped after adding 1 Mb to the start and end locations of each gene. For the second criterion, only peaks that contained fewer than 25 genes and were smaller than 10 Mb were considered.

RNA sequencing for expression and fusion analyses. Of the 1,144 tumors examined in this study, 495 lung ADCs and 476 lung SqCCs had corresponding RNA-seq data from TCGA. RNA reads were generated, aligned to the hg19 genome assembly with Mapsplice[58], and normalized with RSEM[59] to FPKM expression estimates, as previously described[6]. Expression values less than 1 FPKM were set to 1, and all data were $\log_2$ transformed. Skipping of *MET* exon 14 was identified with juncBASE[60] as previously described[6]. Lists of fusions were obtained from previous studies[6,31,61]. Fusions for additional tumors were identified with the PRADA pipeline[62]. To plot the exonic expression of fusion transcripts, exon expression levels were measured and normalized to RPKM values, as previously described[6]. Expression for an individual exon was first z score transformed across all tumors within each tumor type. Subsequently, all exons for a gene were z score transformed again within each tumor. The transcript annotations used for this analysis included ENST00000397752 for *MET*, ENST00000361183 for *CAPZA2*, ENST00000302418 for *KIF5B*, ENST00000323115 for *NTRK2*, ENST00000343526 for *TRIM24*, and ENST00000354600 for *TP63*.

Identification of mutational signatures. NMF was used to deconvolute a $K \times G$ matrix of mutation catalogs into a $K \times N$ matrix of mutational processes and an $N \times G$ matrix of mutational exposures (where G is the number of lung cancer exomes, K is the number of mutational states, and N is the number of estimated mutational processes)[16]. Code for NMF was obtained from MATLAB Central (see URLs) and run using the nnmf function from the MATLAB Statistics Toolbox. We used 6 mutation types with 16 different trinucleotide contexts and 2 transcriptional strands, for a total of 192 mutational states. The number of possible signatures was varied from one to ten, and signature stability was assessed via bootstrapping as previously described[16]. Within each tumor, the fraction of estimated mutations for a signature was derived by dividing the number of estimated mutations for that signature by the sum of the estimated mutations from all signatures.

Predicting immunogenicity. HLA alleles were called with POLYSOLVER[47] for all lung cancer exomes. For each tumor, epitope predictions were made by considering interaction between confidently called HLA alleles and single-residue missense alterations. Separate lists were generated consisting of wild-type and mutant peptides of 8, 9, 10, and 11 amino acids in length, as these are known to be the possible lengths for peptides presented by human MHC class I molecules[63]. We then predicted MHC binding affinity for each of the peptides as described previously[48]. First, a proteasome processing score was calculated using the NetChop program[64]. Then, we used the NetMHC[65], NetMHCpan[66], SMM[67], and SMMPMBEC[68] methods to predict MHC binding affinity values for each peptide and used the median value across all algorithms as a composite measure of binding strength. We also defined the neoepitope ratio for each mutant and wild-type peptide pair as the median affinity value for the mutant peptide divided by the median affinity value for the wild-type peptide. This value was found to be a reliable comparator of the relative immunogenicities of the mutant versus wild-type peptide sequences[48]. Peptide pairs were further considered if the mutant peptide displayed a processing score ≥0.7, a median affinity value ≥0.01, and a neoepitope ratio ≥1 and the mRNA transcript of the gene was expressed in the RNA-seq data for that tumor (among the 15,000 most highly expressed genes in each tumor). Because epitope binding is HLA dependent, the previous steps were performed for each of the called MHC I proteins. After this, only peptides predicted to be the best epitopes for each mutation were considered.

Statistical comparisons. Nonparametric tests such as the Wilcoxon rank-sum test (comparison between two groups) or the Kruskal–Wallis test (comparison between more than two groups) were used for continuous variables unless otherwise noted. The Fisher's exact test was used when comparing two categorical variables. In total, longitudinal data on survival were available for 481 patients with lung ADC and 473 patients with lung SqCC from TCGA. The Cox proportional hazards model was used to examine associations between patient survival and mutation status, with and without controlling for tumor stage. Correction for multiple-hypothesis testing was performed with the Benjamini–Hochberg procedure.

Sample collection and pathology review. Clinical and molecular data from Imielinski *et al.*[8] are available in the database of Genotypes and Phenotypes (dbGaP) under accession phs000488.v1.p1.

52. DePristo, M.A. *et al.* A framework for variation discovery and genotyping using next-generation DNA sequencing data. *Nat. Genet.* **43**, 491–498 (2011).
53. Cibulskis, K. *et al.* ContEst: estimating cross-contamination of human samples in next-generation sequencing data. *Bioinformatics* **27**, 2601–2602 (2011).
54. Carter, S.L. *et al.* Absolute quantification of somatic DNA alterations in human cancer. *Nat. Biotechnol.* **30**, 413–421 (2012).
55. Cibulskis, K. *et al.* Sensitive detection of somatic point mutations in impure and heterogeneous cancer samples. *Nat. Biotechnol.* **31**, 213–219 (2013).
56. Olshen, A.B., Venkatraman, E.S., Lucito, R. & Wigler, M. Circular binary segmentation for the analysis of array-based DNA copy number data. *Biostatistics* **5**, 557–572 (2004).
57. Mermel, C.H. *et al.* GISTIC2.0 facilitates sensitive and confident localization of the targets of focal somatic copy-number alteration in human cancers. *Genome Biol.* **12**, R41 (2011).
58. Wang, K. *et al.* MapSplice: accurate mapping of RNA-seq reads for splice junction discovery. *Nucleic Acids Res.* **38**, e178 (2010).
59. Li, B. & Dewey, C.N. RSEM: accurate transcript quantification from RNA-Seq data with or without a reference genome. *BMC Bioinformatics* **12**, 323 (2011).
60. Brooks, A.N. *et al.* Conservation of an RNA regulatory map between *Drosophila* and mammals. *Genome Res.* **21**, 193–202 (2011).
61. Yoshihara, K. *et al.* The landscape and therapeutic relevance of cancer-associated transcript fusions. *Oncogene* **34**, 4845–4854 (2015).
62. Torres-García, W. *et al.* PRADA: pipeline for RNA sequencing data analysis. *Bioinformatics* **30**, 2224–2226 (2014).
63. Alberts, B. *Molecular Biology of the Cell* (Garland Science, 2002).
64. Nielsen, M., Lundegaard, C., Lund, O. & Keşmir, C. The role of the proteasome in generating cytotoxic T-cell epitopes: insights obtained from improved predictions of proteasomal cleavage. *Immunogenetics* **57**, 33–41 (2005).
65. Nielsen, M. *et al.* Reliable prediction of T-cell epitopes using neural networks with novel sequence representations. *Protein Sci.* **12**, 1007–1017 (2003).
66. Hoof, I. *et al.* NetMHCpan, a method for MHC class I binding prediction beyond humans. *Immunogenetics* **61**, 1–13 (2009).
67. Peters, B. & Sette, A. Generating quantitative models describing the sequence specificity of biological processes with the stabilized matrix method. *BMC Bioinformatics* **6**, 132 (2005).
68. Kim, Y., Sidney, J., Pinilla, C., Sette, A. & Peters, B. Derivation of an amino acid similarity matrix for peptide: MHC binding and its application as a Bayesian prior. *BMC Bioinformatics* **10**, 394 (2009).

doi:10.1038/ng.3564